Expression of membrane-associated proteins within single emulsion cell facsimiles

Analyst

www.rsc.org/analyst

Volume 137 | Number 13 | 7 July 2012 | Pages 2905–3180

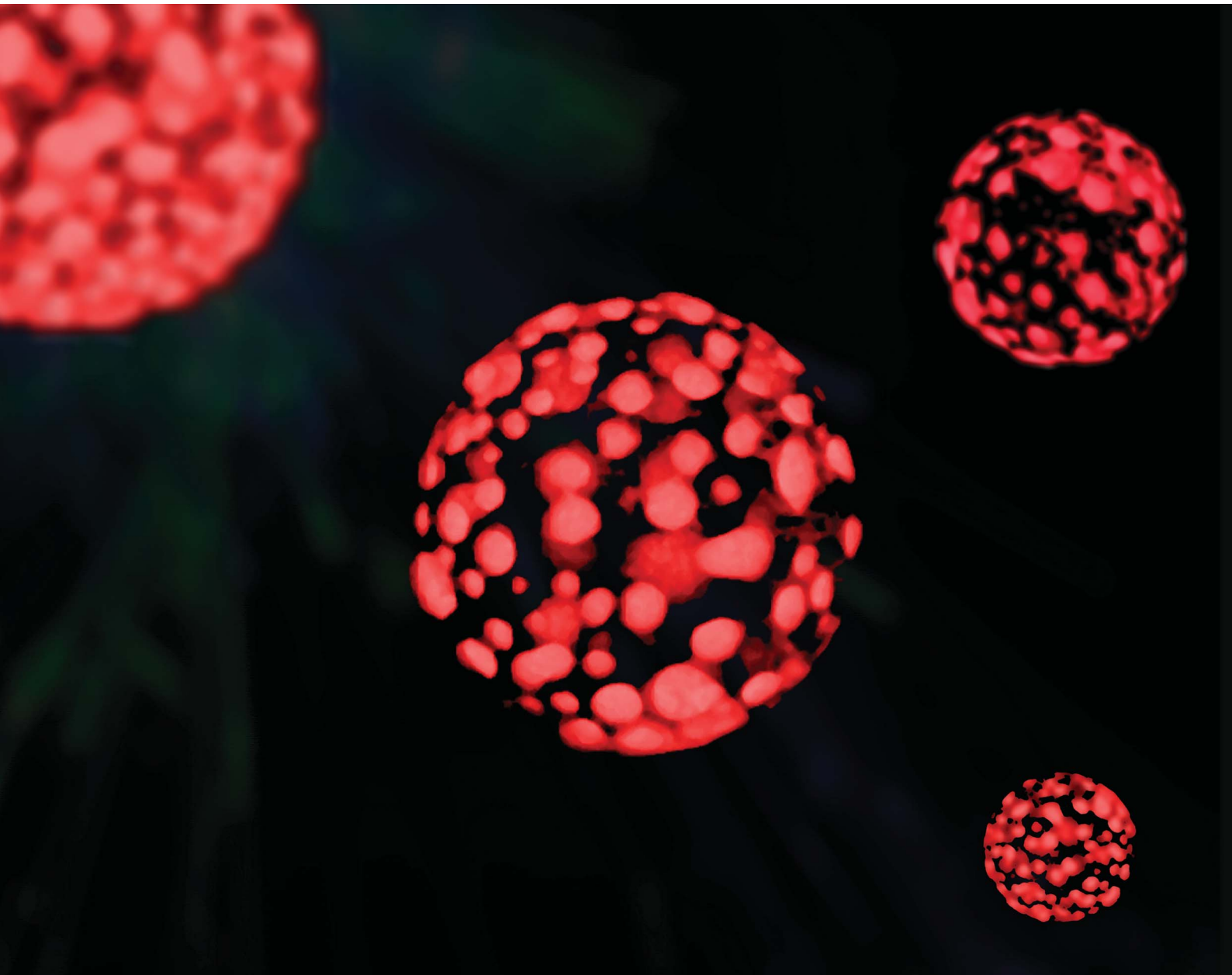

Themed Issue on Single Entities

ISSN 0003-2654

RSC Publishing

HOT ARTICLE
Jonathan M. Cooper *et al.*
Expression of membrane-associated protein within single emulsion cell facsimiles

0003-2654(2012)137:13;1-3

Analyst

Dynamic Article Links

Cite this: *Analyst*, 2012, **137**, 2939

www.rsc.org/analyst

PAPER

Expression of membrane-associated proteins within single emulsion cell facsimiles†

Mayuree Chanasakulniyom,[a] Chiara Martino,[a] David Paterson,[a] Louise Horsfall,[b] Susan Rosser[b] and Jonathan M. Cooper*[a]

Received 10th January 2012, Accepted 2nd March 2012
DOI: 10.1039/c2an35047e

MreB is a structural membrane-associated protein which is one of the key components of the bacterial cytoskeleton. Although it plays an important role in shape maintenance of rod-like bacteria, the understanding of its mechanism of action is still not fully understood. This study shows how segmented flow and microdroplet technology can be used as a new tool for biological *in vitro* investigation of this protein. In this paper, we demonstrate cell-free expression in a single emulsion system to express red fluorescence protein (RFP) and MreB linked RFP (MreB–RFP). We follow the aggregation and localisation of the fusion protein MreB–RFP in this artificial cell-like environment. The expression of MreB–RFP in single emulsion droplets leads to the formation of micrometer-scale protein patches distributed at the water/oil interface.

1. Introduction

Over the last decade, numerous studies have demonstrated the unique contribution that microdroplet technology offers in biological and chemical investigations.[1–3] These methods have generally been implented within segmented flow microfluidic systems, resulting from the introduction of an aqueous phase into a continuous oil phase, which can produce microdrops at rates in excess of 1000 s^{-1}. The impact of the technology is related to the small reaction volumes (ranging from 10^{-9} L to 10^{-15} L) with associated short diffusion distances. This, coupled with advection within the droplets as they pass through microfluidic systems, results in decreased times for reactions, when compared to conventional techniques.[4] The small volumes are also associated with high local concentrations of reactants, even when absolute quantities are small, leading to reduced reagent costs.

Microfluidic technology enables scientists to manipulate droplets in a controlled manner (providing tools that allow merging, splitting, and sorting). Several detailed literature reviews of microdroplet applications have been published detailing how the technology has begun to impact in the cosmetics, pharmaceutical and food industries.[5–8]

Methods involved with combining microdroplet technologies with synthetic biology techniques have proved particularly challenging and innovative.[9–17] Customised DNA templates and commercially available cell-free expression systems have been combined and encapsulated in microdroplets for the synthesis of enzyme and water soluble proteins, such as green fluorescent protein (GFP) and red shifted GFP (rsGFP) .[13–17]

Developments in synthetic biology have potential applications in the construction of artificial cells and more broadly in the production of synthetically created biological structures in artificial environments, like single-emulsion droplets. These constructs, commonly known as water-in-oil or W/O microdrops provide a tool which enables study of biological components in isolation, or can be used to transplant useful biological pathways into an easily controlable experimental platform to achieve a specific goal. For example, during the manufacture of drugs or biofuels, reactions can be carried out in a droplet microreactor possessing many of the physiochemical properties of *in vivo* cells (it is of a similar size to a cell and has a hydrophobic/hydrophilic interface with a similar curvature of a cell).

In this paper, we demonstrate the combination of microdropet technology with cell-free protein expression for the production of a structural membrane-associated protein (MreB) within an artificial compartment. The single emulsion system offers an ideal model to express the protein and to observe its behavior in a cell-like system.

MreB is a bacterial actin homologue protein, which assembles in bacterial cytoplasmatic filaments lying just underneath the membrane. Its primary function is to organize the cell wall synthesis machinery,[18] but MreB also plays an important role in the maintenance of shape in rod-like bacteria, *e.g. E. coli.*[19,20] Recently it has been discovered that the origin of MreB's

[a]*The Division of Biomedical Engineering, School of Engineering, The University of Glasgow, G12 8LT Glasgow, UK. E-mail: jon.cooper@glasgow.ac.uk; Fax: +44 (0)141-330-4907*
[b]*The Institute of Molecular Cell and System Biology, College of Medical and Veterinary and Life Science, The University of Glasgow, G12 8QQ Glasgow, UK*

† This article is part of a themed issue highlighting the targeted study of single units, such as molecules, cells, organelles and pores—The "Single" Issue, guest edited by Henry White.

membrane binding activity results from the presence of an *N*-terminal amphipathic helix.[18] Although scientists have proved that MreB is responsible for bacterial elongation, the process by which a bacterial cell becomes rod-shaped and a complete understanding of its mechanism of action remain poorly understood.[21,22]

To gain a better understanding of the role of MreB, scientists have used many different methods of investigation to study its structure, function and distribution, including site directed mutagenesis, immunocytochemical fluorescence staining with fluorescence microscopy, drug treatment and biophysical simulation.[18–22] In this paper, we now propose the use of microdroplet technology as a possible new tool for biological *in vitro* investigation of this protein. We show the cell-free production of this structural protein, and study the dynamics of the expression process, leading to the formation of micometer scale protein patches distributed at the interface water/oil.

2. Experimental

2.1 Microfluidic droplet generator

The droplet-based microfluidic device was designed and fabricated using standard soft lithographic techniques. Schematic representation of the device is given in Fig. 1. The upper part of device was made from PDMS (Sylgard 184, Dow Corning) casted on a silicon master structure. The silicon master itself was fabricated using standard photolithographic processing including pattern transfer and dry etching. Details of the device fabrication can be found in our previous studies, involving microdroplets including, for example.[23]

2.2 Plasmid construction

BioBrick ref BBa_I719015 was obtained from the Registry of Standard Biological Parts, which contains gene expression cassette of T7 promoter–RBS–mGFP–terminator in pSB1A2. This plasmid was reconstructed as pB1A2_BX by introducing *Bam*HI and *Xho*I sites between the RBS and terminator instead of m*GFP* gene. *MreB* gene was PCR-amplified from the genomic DNA isolated from *E. coli* strain KO11 using the TIANamp bacteria DNA kit (Tiangen, China). The reporter gene *RFP* was amplified from BioBrick BBa_E1010, using RFP_forward and RFP_reverse primers. The fusion protein gene *MreB–RFP* was assembled by overlap extension PCR, with GS linker inserted between the two genes. Then the *MreB–RFP* fragment was inserted into pSB1A2_BX with *Bam*HI and *Xho*I, resulting in the vector pSB1A2_BX(*MreB–RFP*), which contains the target gene expression cassette T7 promoter–RBS–*MreB–RFP*–terminator.

The fusion protein gene *MreB–RFP* with GS linker and the *RFP* gene alone were PCR-amplified from plasmid pSB1A2_BX(*MreB–RFP*) using Platinum® Taq DNA Polymerase High Fidelity (Invitrogen, UK) and primers MreB_NT_for and MreB_NT_rev or RFP_NT_for and MreB_NT_rev. The general protocol for the polymerase was followed with an additional final 30 min extension step at 68 °C. After gel extraction (Qiagen, UK) the PCR products were used in pEXP5-NT/TOPO® Cloning reactions (Invitrogen, UK) to obtain the plasmid pMreB-NT containing the *N*-terminal His_6 tagged fusion protein gene *MreB–RFP* with GS linker and the control plasmid pRFP-NT containing the *RFP* gene with an *N*-terminal His_6 tag.

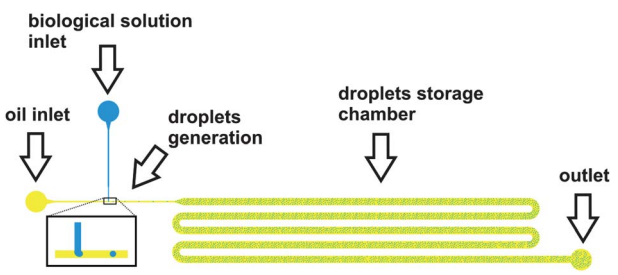

Fig. 1 Geometry of microfluidic device for W/O droplet generation. The chip comprised two inlets for injection of two immiscible phases, a serpertine chamber where droplets were stored and imaged and an outlet useful for droplet collection outside the chip. The channel was created in PDMS with height and width of 100 μm.

2.3 MreB–RFP and RFP cell-free expression

E. coli extract and all solutions containing the biological machinery for protein synthesis were purchased as a ribosomal cell free extract from Invitrogen in the Expressway™ Cell-Free *E. coli* Expression System. Following the manufacturer supplied protocol, 1 μg of DNA plasmid was first mixed with *E. coli* extract, T7 Enzyme mix, 75 mM methionine, 50 mM amino acid, RNase-free distilled water. The solution was then mixed with a feeding solution containing 75 mM methionine, 50 mM amino acid, RNase-free distilled water. This was loaded into a 100 ml glass syringe (Hamilton) and connected to the device.

To observe the dynamics of MreB–RFP and RFP cell-free protein expression, single emulsion devices comprising of 2 inlets were used. One inlet was used for the continuous fluorinated oil phase with 2% EA surfactant (Raindance Technologies), while the other inlet was used for the ribosomal cell-free extract. Both the oil–surfactant solution and cell-free reaction were introduced into the devices *via* syringe pump (Harvard Apparatus) at initial flow rates of 1 μl min^{-1}. The flow rate was subsequently reduced to 0.5 μl min^{-1} after the droplets were being constantly generated.

MreB–RFP and RFP protein expression in the droplets was monitored using time lapse fluorescence microscopy (Axiovert 200 microscope, Carl Zeiss) at 32 °C. Images were captured every 10 min in the first 6 h and every 30 min for 6 h afterwards. The mean fluorescent intensities were quantified using ImageJ and expressed as a function of time. The relative protein expression of both MreB–RFP and RFP at each time point were normalised against the initial background fluorescence intensities at droplet formation, and were expressed in arbitrary units.

2.4 Confocal image

Ziess LSM 510 META microscope (Carl Zeiss Ltd., Welwyn Garden City) was used to collect the fluorescence images, using a Ziess LD-Plan Neofluor 40×/0.6 Korr objective. The data acquisition and signal processing were controlled by the supplied Ziess software. Micrographs of MreB–RFP patches were obtained using inbuilt digital zoom feature.

3. Results and discussion

3.1 MreB–RFP and RFP expression

Both the structural fusion protein (MreB–RFP) and the water soluble protein (RFP), used as a control, were expressed in single emulsion droplets. Increases in RFP fluorescence indicated successful expression of fusion protein MreB–RFP by cell-free expression. Droplets containing MreB–RFP showed the formation of MreB–RFP aggregates at the water/oil interface after 24 hours of incubation (Fig. 2A) while the RFP protein remained homogeneously dispersed in solution (Fig. 2B). The dynamics of Mreb–RFP and RFP expression are shown in Fig. 2C. The fluorescence intensities of MreB–RFP and RFP at each time point were normalised with their fluorescence intensities at the starting point (10 different droplets were measured, $n = 10$). Fluorescence intensities showed a trend that increased over time. The expression rate of RFP was higher than MreB–RFP, showing approximately five-fold greater expression. The larger DNA template for MreB–RFP with respect to RFP (1726 base pairs compared to 675 base pairs) may account for the increased expression rate of the smaller RFP template. Increased coding length will result in slower transcription, and the slower diffusion of the larger template within the microdroplet, leading to increase time intervals between transcription events.

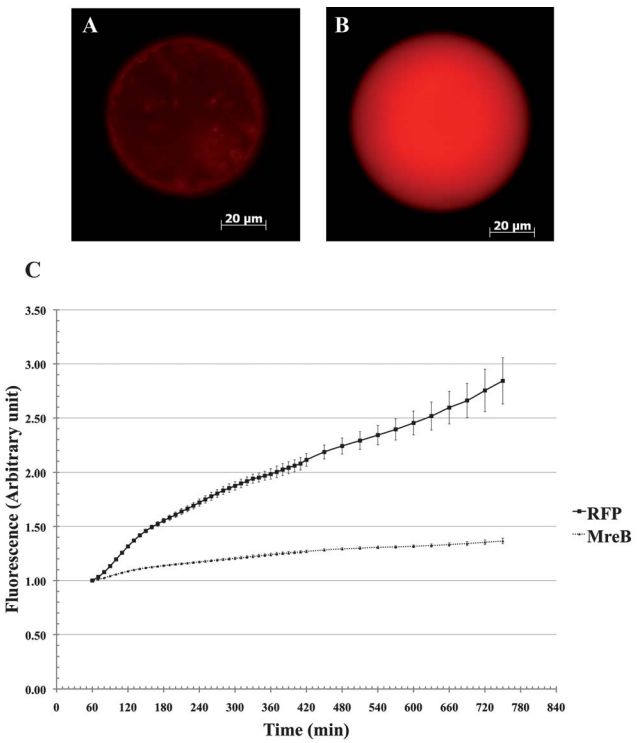

Fig. 2 Cell-free MreB–RFP and RFP expression in single emulsion. The fluorescence images of droplets expressing MreB–RFP and RFP were acquired 24 hours after starting the reaction (incubated at 32 °C). MreB–RFP forms aggregates localised at the water/oil interface (A) while the RFP protein remained dispersed throughout the droplet (B). The relative protein expression of both MreB–RFP and RFP showed a trend that increased with time (C). The fluorescence intensities of MreB–RFP and RFP at each time point were normalised with their fluorescent intensities at the starting point ($n = 10$).

The mRNA levels correspond to protein expression. Differences in protein concentrations are 20–40% of those attributed to mRNA levels.[24,25] In addition to mRNA levels, ribosome density (the number of ribosomes on active mRNAs normalised by transcript length) may also play a role in the production of proteins. The longer those transcripts are, the slower the translation process will be. Moreover, the long transcripts require a number of bound ribosomes to produce new proteins, which also effects the synthesis rate.[26] In addition to the size of the encoding sequence, conformation change of RFP might have an impact on the fluorescence intensity of the MreB–RFP fusion protein. The fusion protein might cause structural hindrance or misfolding to RFP that affect RFP intensity.

3.2 MreB–RFP aggregates at the interface

Fig. 3A–C shows confocal Z-stack images of a single emulsion droplet containing MreB–RFP aggregates (bottom, equatorial and top view). The images revealed that cell-free production of MreB–RFP in microdroplets led to the formation of ~3 μm diameter patch-like aggregates distributed at the water/oil interface (Fig. 3D and E). The distribution of MreB at the interface might be affected by its structure. MreB has an *N*-terminal amphipathic helix that binds directly to cell membrane. The binding is relatively strong due to the hydrophobicity of the amphipathic helix. A stable mutant of *E. coli* MreB lacking the *N*-terminal amphipathic helix does not bind strongly to membrane while the wild-type *E. coli* MreB does.[18] One implication is that once the MreB–RFP adsorbs at the water/oil interface, it might be difficult to dissociate from the interface.

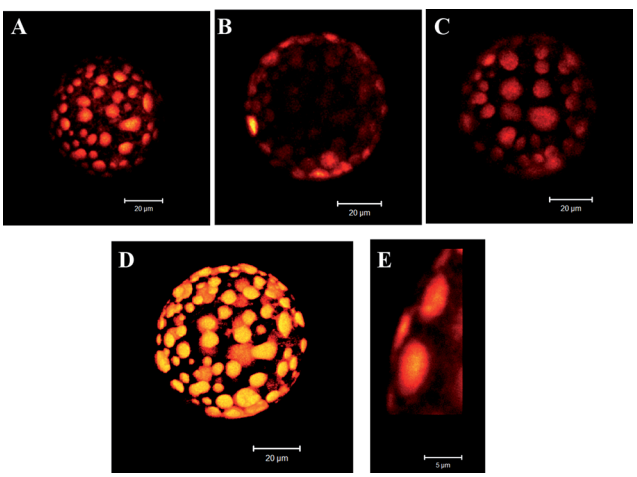

Fig. 3 Confocal images of MreB–RFP protein patch formation in microdroplets after 24 hours of incubation. (A) Bottom view of a single emulsion droplet containing MreB–RFP aggregates; (B) equatorial cross-section of the droplet, showing the localisation of the MreB–RFP patches to the interfacial region; (C) top view of the single emulsion droplet containing MreB–RFP aggegates. Scale bar = 20 μm; (D) reconstructed 3D model of a microdrop with a MreB–RFP aggregate, constructed from confocal z-stack. Scale bar = 20 μm; (E) close-up of MreB–RFP patch showed the average size of patches within the droplets was approximately 3 μm (E). Scale bar = 3 μm.

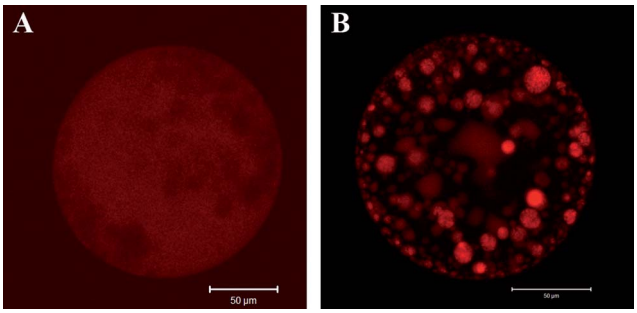

Fig. 4 MreB–RFP patches formation in large droplets. Cross-section images of single emulsion droplets ~150 μm in diameter were taken after 24 hours (A) and 96 hours (B) of incubation. Scale bar = 50 μm.

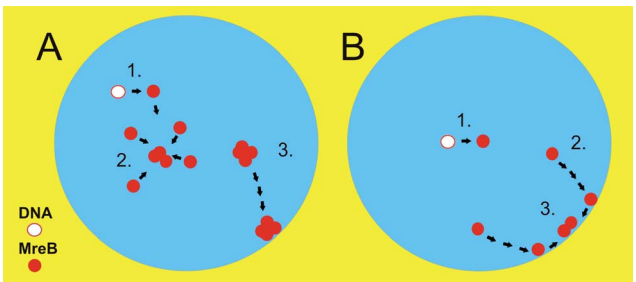

Fig. 5 Possible mechanisms of patch formation within the microdroplet: (A) after the protein monomers are synthesized (1), they might aggregate (2) and then migrate to the water/oil interface (3); (B) After protein synthesis (1) the monomers migrate to the interface (2) where the polymerisation and patches formation are initiated (3).

3.3 Formation of MreB–RFP aggregates

The formation of MreB–RFP aggregates depended upon droplet size and incubation time. Droplets with small size (≤50 μm in diameter) showed the formation of MreB–RFP aggregates after 24 hours of incubation (Fig. 3), while the MreB–RFP protein remains dispersed in solution within droplets larger than 50 μm in diameter (Fig. 4A). For larger droplets, it took about 96 hours to form aggregates similar to those seen in smaller droplets (Fig. 4B). The surface area to volume ratio might account for the heterogeneous kinetics of patch formation in different sizes of droplets; the larger surface area to volume ratios for smaller droplets leading to shorter diffusion times to the interface.

There are two possible hypotheses that could explain the formation of aggregates. First, the MreB–RFP monomers aggregate and form a polymer before moving to the interface (Fig. 5A). Monomer binding to the interface could be prevented prior to polymerization, if the amino acid residues comprising the amphipathic membrane-binding helix are sequestered within MreB's 3D protein structure. The helix could be released by morphological changes induced in the monomer during the process of polymerization. Alternatively, the monomers adhere to the interface prior to aggregation to form a larger polymer (Fig. 5B). Adhesion of the monomers to the interface might be another phenomenon to obscure the hydrophobic part from the aqueous medium before forming the aggregation. However, these two possible hypotheses require further investigation.

Conclusions

We demonstrate the combination of microdroplet technology with cell-free protein expression in order to examine the aggregation and localisation of MreB, a prokaryotic membrane-associated protein within a cell-like facsimile. The aggregation kinetics depend on droplet size, with aggregates showing a preference for localisation at the water/oil interface, consistent with expectations. Results obtained show the stability of the W/O droplets, the homogeneity of distribution of RFP and aggregation of MreB at the W/O interface, indicating that single emulsion microdroplets are an interesting experimental platform for the study of biological systems. Continuing experiments in this area show the potential to elucidate the mechanism of this action of this protein, revealing how it exercises control over bacterial cell morphology.

Acknowledgements

The authors are grateful to BBSRC and The Royal Thai Government Science and Technology Scholarship for support of the work. Other aspects of the work were also supported EPSRC DTC, The University of Glasgow, School of Engineering and The Department of Pharmaceutical Engineering of Tianjin University. The authors also thank Niall Macdonald for contribution to this work.

Notes and references

1 W. T. S. Huck, A. B. Theberge, F. Courtois, Y. Schaerli, M. Fischlechner, C. Abell and F. Hollfelder, *Angew. Chem., Int. Ed.*, 2010, **49**, 5846–5868.
2 A. B. Theberge, F. Courtois, Y. Schaerli, M. Fischlechner, C. Abell, F. Hollfelder and W. T. S. Huck, *Angew. Chem., Int. Ed.*, 2010, **49**, 5846–5868.
3 A. P. Lee, S. Y. Teh, R. Lin and L. H. Hung, *Lab Chip*, 2008, **8**, 198–220.
4 X. C. I. Solvas and A. deMello, *Chem. Commun.*, 2011, **47**, 1936–1942.
5 N. Pannacci, H. Bruus, D. Bartolo, I. Etchart, T. Lockhart, Y. Hennequin, H. Willaime and P. Tabeling, *Phys. Rev. Lett.*, 2008, **101**, 164502-1–164502-4.
6 A. S. Utada, E. Lorenceau, D. R. Link, P. D. Kaplan, H. A. Stone and D. A. Weitz, *Science*, 2005, **308**, 537–541.
7 S. Okushima, T. Nisisako, T. Torii and T. Higuchi, *Langmuir*, 2004, **20**, 9905–9908.
8 D. A. Weitz, R. K. Shah, H. C. Shum, A. C. Rowat, D. Lee, J. J. Agresti, A. S. Utada, L. Y. Chu, J. W. Kim, A. Fernandez-Nieves and C. J. Martinez, *Mater. Today*, 2008, **11**, 18–27.
9 D. S. Tawfik and A. D. Griffiths, *Nat. Biotechnol.*, 1998, **16**, 652–656.
10 P. Schwille and S. Diez, *Crit. Rev. Biochem. Mol. Biol.*, 2009, **44**, 223–242.
11 N. Szita, K. Polizzi, N. Jaccard and F. Baganz, *Curr. Opin. Biotechnol.*, 2010, **21**, 517–523.
12 A. J. Demello, S. Gulati, V. Rouilly, X. Z. Niu, J. Chappell, R. I. Kitney, J. B. Edel and P. S. Freemont, *J. R. Soc., Interface*, 2009, **6**, S493–S506.
13 C. Martino, L. Horsfall, Y. Chen, M. Chanasakulniyom, D. Paterson, A. Brunet, S. Rosser, Y.-J. Yuan and J. M. Cooper, *ChemBioChem*, 2012, submitted.
14 P. S. Dittrich, M. Jahnz and P. Schwille, *ChemBioChem*, 2005, **6**, 811.
15 F. Courtois, L. F. Olguin, G. Whyte, D. Bratton, W. T. S. Huck, C. Abell and F. Hollfelder, *ChemBioChem*, 2008, **9**, 439–446.
16 Y. Zhu, N. Wu, J. G. Oakeshott, C. J. Easton, T. S. Peat and R. Surjadi, *J. Micromech. Microeng.*, 2011, **21**, 054032-1–054032-7.
17 Y. G. Zhu, N. Wu, F. Courtois, R. Surjadi, J. Oakeshott, T. S. Peat, C. J. Easton and C. Abell, *Eng. Life Sci.*, 2011, **11**, 157–164.

18 J. Salje, F. van den Ent, P. de Boer and J. Löwe, *Mol. Cell*, 2011, **43**, 478–487.
19 J. Errington, L. J. F. Jones and R. Carballido-Lopez, *Cell*, 2001, **104**, 913–922.
20 D. Popp, A. Narita, K. Maeda, T. Fujisawa, U. Ghoshdastider, M. Iwasa, Y. Maeda and R. C. Robinson, *J. Biol. Chem.*, 2010, **285**, 15858–15865.
21 K. D. Young, *Annu. Rev. Microbiol.*, 2010, **64**, 223–240.
22 S. van Teeffelen, S. Wang, L. Furchtgott, K. C. Huang, N. S. Wingreen, J. W. Shaevitz and Z. Gitai, *Proc. Natl. Acad. Sci. U. S. A.*, 2011, 15822–15827.
23 C. Martino, M. Zagnoni, M. E. Sandison, M. Chanasakulniyom, A. R. Pitt and J. M. Cooper, *Anal. Chem.*, 2011, **83**, 5361–5368.
24 L. Nie, G. Wu and W. Zhang, *Biochem. Biophys. Res. Commun.*, 2006, **339**, 603–610.
25 Q. Tian, S. B. Stepaniants, M. Mao, L. Weng, M. C. Feetham, M. J. Doyle, E. C. Yi, H. Dai, V. Thorsson, J. Eng, D. Goodlett, J. P. Berger, B. Gunter, P. S. Linseley, R. B. Stoughton, R. Aebersold, S. J. Collins, W. A. Hanlon and L. E. Hood, *Mol. Cell. Proteomics*, 2004, **3**, 960–969.
26 R. Brockmann, A. Beyer, J. J. Heinisch and T. Wilhelm, *PLoS Comput. Biol.*, 2007, **3**, e57.